

RESEARCH

Open Access



Therapeutic potential of total flavonoids of *Rhizoma Drynariae*: inhibiting adipogenesis and promoting osteogenesis via MAPK/HIF-1 α pathway in primary osteoporosis

Hui Su^{1†}, Luyao Liu^{1†}, Zechen Yan¹, WenXuan Guo², Guangxin Huang³, Rujie Zhuang^{1,2,4*} and Yu Pan^{2*}

Abstract

Aim This study seeks to confirm the therapeutic effectiveness of TRFD in inhibiting adipogenesis and promoting osteogenesis in primary osteoporosis through the MAPK/HIF-1 α signaling pathway. C57BL/6J mice underwent ovariectomy (OVX) to induce osteoporosis. Mice were administered TRFD (Low and high doses) estradiol for a duration of 12 weeks. Bone microarchitecture evaluated using Micro-CT, while serum biomarkers and protein expressions were analyzed through enzyme-linked immunosorbent assay, Western blotting, and immunohistochemistry. Furthermore, BMSC were isolated to show differentiation, Osteogenic and adipogenic induction were performed, including ALP activity and Oil Red O staining. Bioinformatics analysis of RNA sequencing data was conducted to identify differentially expressed genes.

Results Total flavonoids of *Rhizoma Drynariae* treatment significantly improved bone microarchitecture and reversed histopathological damage in OVX mice. It increased serum levels of osteogenesis markers (RUNX2, BMP-2) and enhanced MAPK and HIF-1 α signaling pathways, The results also showed a significant dose, TFDR enhanced the osteogenic differentiation of BMSCs while suppressing adipogenic differentiation, as demonstrated by increased ALP activity and mineralization, alongside, the expression of lipid markers (PPAR- γ , C/EBP α) was inhibited. Furthermore, MAPK/HIF-1 α pathway was confirmed be crucial in mediating these effects.

Conclusion TRFD exhibits significant therapeutic potential in treating primary osteoporosis by promoting osteogenesis and inhibiting adipogenesis through the MAPK/HIF-1 α pathway. These establish an investigation of TRFD as a natural treatment option for managing osteoporosis.

Clinical trial number Not applicable.

[†]Hui su and Luyao Liu contributed equally to this work.

*Correspondence:

Rujie Zhuang
rujiezhuang@163.com

Yu Pan
panyu9022@163.com

Full list of author information is available at the end of the article



Keywords Rhizoma drynariae (*Drynaria fortunei* J. Smith), Total flavonoids, Osteoporosis, MAPK, HIF-1 α , Adipogenesis, Osteogenesis

Introduction

Osteoporosis [1, 2], marked by low bone mass, microstructural degeneration of bone. Effective prevention and treatment strategies are essential to manage osteoporosis and reduce its impact on individuals and health-care systems. It is a complex, multifactorial disorder associated with various risk factors and medical conditions [3–5]. Osteoblasts, the primary cells responsible for bone formation, differentiate and synthesize bone matrix throughout skeletal development. This differentiation process usually advances through stages involving mesenchymal progenitors, preosteoblasts, and mature osteoblasts [6, 7]. Over decades of study, it has become increasingly clear that the adipogenesis and osteogenesis of MSCs are competitive and reciprocal processes [8, 9]. Adipocytes, which make up 15–70% in the bone micro-environment, which is often linked to undergo variations in both number and size with aging and in various clinical conditions associated with bone loss, such as osteoporosis [10]. As a result, significant focus has been placed on studying how bone marrow adipocytes affect bone remodeling and their connection to disorders associated with bone loss. Bone marrow mesenchymal stem cells (MSCs) are pluripotent stem cells that can differentiate into either adipocytes or bone-forming osteoblasts. Research has indicated that adipocytes adjust the differentiation [11, 12].

Numerous critical factors regulate bone development and maintain bone homeostasis in bone loss. Runx2 (Runt-related transcription factor 2) [13] is a master regulator crucial for osteoblast differentiation and bone formation. It activates the expression of multiple genes involved in osteogenesis, including collagen and osteocalcin. During normal bone development and maintenance, high Runx2 expression promotes osteoblast formation while relatively inhibiting adipocyte differentiation. BMP-2 (Bone Morphogenetic Protein-2) [14], acts as a potent inducer of bone formation [15]. Significant and consistent evidence from clinical research suggests that various conditions linked to bone loss, including osteoporosis, aging, and glucocorticoid therapy, are commonly linked to a rise in fat tissue within the bone marrow. Studies have shown that Wnt signaling pathways diminish the expression and activity of influential adipogenic transcription factors, including peroxisome proliferator-activated receptor γ (PPAR γ) and enhancer-binding protein α (C/EBP α), thus inhibiting the formation of adipocytes [16, 17].

Traditional Chinese Medicine provides distinct benefits for the management of osteoporosis, primarily due to

its incorporation of various components and therapeutic targets. As a key component of traditional Chinese medicine, Rhizoma Drynariae (*Drynaria fortunei* J. Smith) has been used for centuries due to its therapeutic properties [18, 19]. According to the *Chinese Pharmacopoeia*, Rhizoma Drynariae (*Drynaria fortunei* J. Smith) has effects such as promoting healing and alleviating pain, tonifying the kidneys and strengthening bones, as well as dispelling wind and reducing spots [20, 21]. It is one of the commonly used traditional Chinese medicines in orthopedics. Modern research shows that the active components of *Dipsacus* mainly include flavonoids, triterpenoids, phenolic acids, steroid compounds, and their glycosides, among which flavonoids have become a key focus of research in recent years [20, 21]. Flavonoid compounds are the primary constituents that exert anti-osteoporotic effects. Its efficacy in preventing and treating osteoporosis has been developed into a Class II new drug (Qianggu Capsules), which has also achieved favorable clinical outcomes [22, 23]. Previous studies showed [24, 25], TFDR demonstrate encouraging pharmacological effects, with the potential to enhance BMD and modify serum levels of ALP, and CTX in mice. Research indicates that TFDR can induce apoptosis in osteoclasts while promoting the proliferation of osteoblasts, contributing to its widespread application in osteoporosis treatment.

The MAPK signaling pathway is activated by external stimuli like cytokines, stress, and growth factors, leading to the phosphorylation and activation of protein kinases such as ERK, JNK, and p38 [26]. In osteoporosis, MAPK signaling regulates osteoblast activity and bone formation. Studies indicate that MAPK activation promotes osteoblast differentiation and proliferation while enhancing bone matrix synthesis [27, 28]. HIF1- α (Hypoxia-Inducible Factor 1- α), a transcription factor stabilized under low oxygen conditions, regulates gene expression related to metabolism, angiogenesis, cell proliferation, and differentiation. In the bone marrow microenvironment, HIF-1 α plays a crucial role in regulating bone and fat production by influencing the differentiation of bone marrow-derived mesenchymal stem cells (BMSCs) [25, 26]. Studies have shown that mice lacking the HIF-1 α gene exhibit significantly reduced bone mineral density [27]. Moreover, the local administration of HIF-1 α mimics in bone defects has been found to enhance callus regeneration and promote osteogenesis, indicating that HIF-1 α is a key regulator of bone metabolism.

Study aim to explore the RDTF for treating primary osteoporosis. Specifically, the study aims to elucidate the mechanisms by which RDTFs inhibit adipogenesis and

promote osteogenesis through the MAPK/HIF1- α signaling pathway. Result show these pathways at the molecular level, contributing to the treatment on bone quality deterioration associated with primary osteoporosis. The methods and experimental design of this study are shown in Fig. 1.

Materials and methods

Animals and treatments

SPF female C57/BL6J mice, aged 6 weeks and weighing approximately 20 \pm 2 g. All experimental procedures involving with the Committee group of Experimental Animal Ethics at Zhejiang Chinese Medical University. All animals were purchased from Beijing Weitonglihua Animal Science and Technology Development SCXK (JING) 2016-0011. The experimental animals were provided by the Animal Experiment Ethics Committee of Zhejiang Chinese Medical University, No. 20231204-04.

Drug administration

50 female mice were randomly separated to four groups: control group, an ovariectomized model group (OVX), sham-operated group (SHAM), an treatment group with estradiol-positive drug group (E2), and total flavonoids of rhizoma drynariae treatment group: Low dose treatment of TRFD group (TRFD-L), High dose treatment of TRFD

group (TRFD-H), with 10 mice in each group. Bilateral ovariectomy was performed on the model group to simulate the sudden decline in estrogen levels observed in postmenopausal women. In the OVX group, an abdominal incision was made to locate the ovaries, which were then completely removed following ligation of the uterine horn, and the incision was sutured. In the SHAM group, only the fat mass near the ovary was removed. Seven days post-operation, mice in OVX and the SHAM were administered distilled water by gavage. The E2 group received estradiol (27.273 mg/kg/day), while the TRFD group was administered Low dose treatment group -TRFD-L 66.4775 mg/kg/day, High dose treatment group - TRFD-H (132.955 mg/kg/day) by gavage. After 12 weeks the next analysis was performed. Estradiol (98% purity, S30633), from Source Leaf; total flavonoids of rhizoma drynariae (total flavonoids content is 98%, Chinese medicine approval number Z20133051), from Beijing Qi Huang Pharmaceutical Co., LTD.

Micro-computed tomography (Micro-CT) scan

The femur of Micro-CT imaging was employed to test the bone structure. The scanning settings were configured at(80 kV;500 μ A), ROI was selected for image from the CT data. The assessed parameters included bone volume relative to total volume (BV/TV), bone surface area

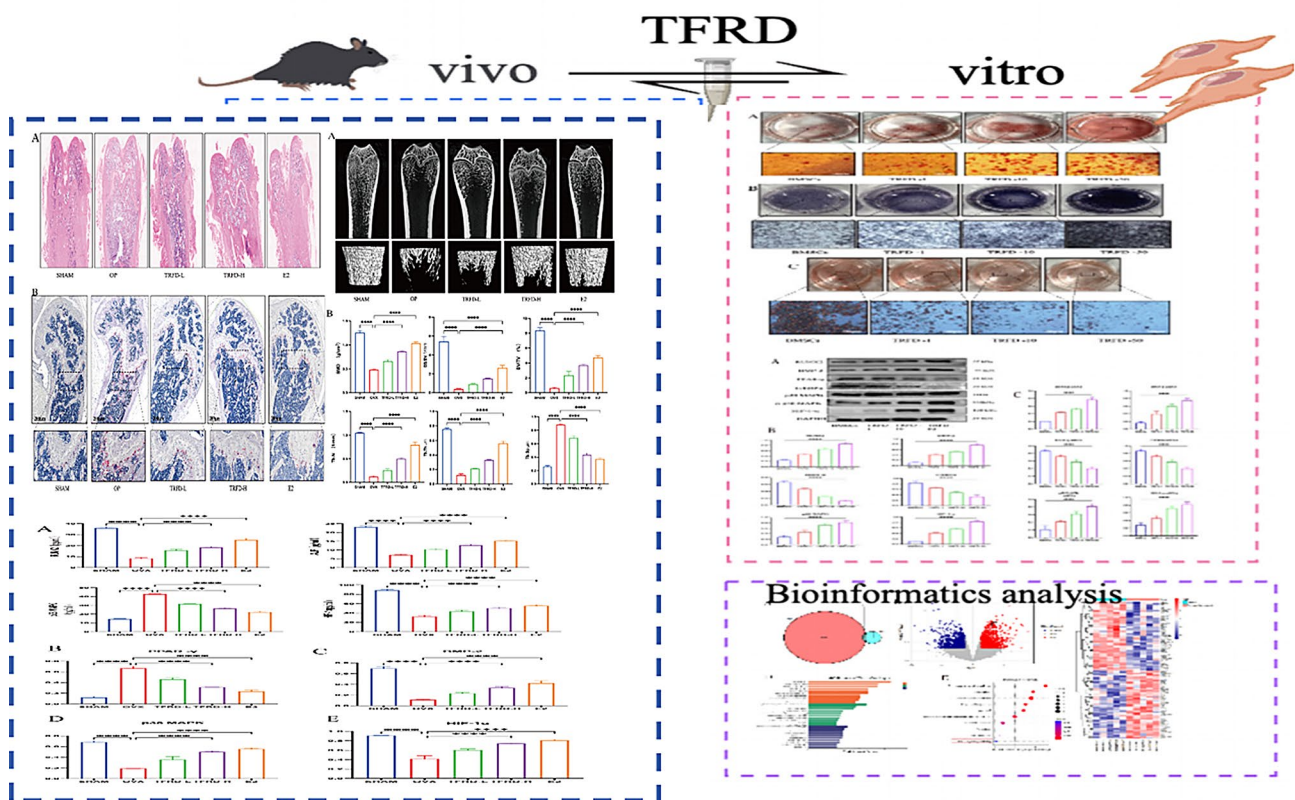


Fig. 1 Overview of the research methodology

in relation to bone volume, trabecular thickness (Tb.Th, mm), and trabecular spacing (Tb.Sp, mm) for comparative record.

Enzyme-linked immunosorbent assay (ELISA)

Levels of cytokines were measured using enzyme-linked immunosorbent assay (ELISA) kits. The concentrations of ALP, RUNX2, p38-MAPK, and HIF-1 α were specifically measured by mouse ELISA kits, with the protocols and recommendations provided by the manufacturer.

Hematoxylin and Eosin (HE) and TRAP staining

The femurs of the mice were treated with paraformaldehyde (4%) by 24 hours. The samples then completely decalcified using 10% ethylenediaminetetraacetic acid and subjected to a dehydration process through ethanol concentrations (50%, 75%, 80%, 85%, 90%, 95%, and 100%). Following this, the bone tissue was made transparent in xylene. All samples sliced into sections that were 5 μ m. Then used for TRAP and HE staining kit, captured using microscope.

Immunohistochemistry and Immunofluorescence

Immunohistochemistry (IHC) staining was conducted using antibodies specific to BMP-2 (1:200, Abcam), MAPK (1:100, Abcam), and HIF-1 α (1:100, Abcam). Then treated with horseradish peroxidase (HRP)-linked secondary antibodies. Following this, the sections underwent staining with a DAB kit, images were captured using a microscope scanner. For immunofluorescence, 4 μ m thick sections from the distal femoral epiphyses that were paraffin-embedded were used. All sections underwent blocking with 500 μ l of blocking solution for 1 h, followed by overnight incubation at 4 $^{\circ}$ C with PPAR- γ antibodies (1:200, Abcam). And then, goat anti-rabbit immunoglobulin G, staining the nuclei with DAPI at a concentration 10 min. Then washed with PBS, and captured using microscope.

Bioinformatics analysis

To investigate the effects of total TRFD on primary osteoporosis, RNA sequencing data from treated and control groups were analyzed for gene expression using the DESeq2 package in R. Genes were considered differentially expressed if they exhibited an adjusted p-value of less than 0.05 and $|\log_2\text{FoldChange}| > 1$. The VennDiagram package in R was utilized to generate a Venn diagram illustrating the overlap between differentially expressed genes. Enrichment analyses for GO and KEGG pathways. This aimed to show enriched biological pathways associated with the differentially expressed genes ($p < 0.05$).

BMSC Preparation and culture

BMSCs were extracted from the SD rats. Under sterile conditions, bone marrow was collected from both femurs. The harvested cells were then seeded into plastic flasks containing DMEM-LG supplemented with 10% fetal bovine serum, 10 ng/ml epidermal growth factor, and antibiotics at 37 $^{\circ}$ C in a humidified atmosphere with 5% CO₂ (Precision Scientific, MA, USA). After 48 h, BMSCs adhered to the flask bottoms. The culture medium was refreshed every 3 to 4 days. Further purification of the cells was achieved through successive passaging.

BMSC osteogenic and adipogenic induction

Osteogenic Induction: When BMSCs reached approximately 80% confluence, they were transitioned to an osteogenic induction medium. This medium comprised DMEM-LG (Gibco, Lot: 12345), 10% fetal bovine serum, β -glycerophosphate, ascorbic acid, and dexamethasone). The cells were incubated at 37 $^{\circ}$ C in a 5% CO₂ environment, with medium changes occurring every three days. Subsequently, osteogenic differentiation was evaluated through ALP staining and Alizarin Red S staining.

Adipogenic Induction: BMSCs cultured to approximately 80% confluence were switched to adipogenic induction medium, which included DMEM-LG, 10% fetal bovine serum, Dexamethasone, 0.5 mM 3-isobutyl-1-methylxanthine, insulin, and 200 μ M indomethacin. Cells were incubated at 37 $^{\circ}$ C in a 5% CO₂ incubator, with the medium changed every 3 days. After 14 days, assessment of adipogenic differentiation was conducted using Oil Red O staining.

Alkaline phosphatase (ALP) activity

ALP activity was assessed using an ALP activity assay kit. After, the cells were washed with PBS and lysed with lysis buffer. Subsequently added substrate solution to the lysates and measured at 405 nm.

Alkaline phosphatase (ALP) staining

ALP staining was conducted using a staining kit based on the azo-coupling method. The ALP incubation solution (with a ratio of AS-BI to FBB of 1:1) was added dropwise, and the mixture was kept in the dark for 20 min. Afterward, the chondrocytes underwent counterstaining with a nuclear fast red solution for a duration of 5 min. Ultimately, the cells were examined using with microscope.

Alizarin red S (ARS) staining

Cells were treated in 10% formaldehyde 15 min. Following the removal of formaldehyde, then rinsed with water and stained with Alizarin Red S. To reduce nonspecific staining, Finally, images of the stained cultures were

taken. Ultimately, the cells were examined using with microscope.

Oil red O (ORO) staining

Cells were fixed in 50% ice-cold ethanol at 4 °C for 30 min and subsequently stained with Oil Red O for 10 min, and the cells were rinsed with 50% ethanol and aqua ad iniectionabilia. Ultimately, the cells were examined using with microscope.

Western blotting (WB) analysis

To assess the protein expression levels in different groups of BMSC cells, we performed Western blot analysis. We extracted total cellular proteins and quantified them using a BCA protein assay kit (Beyotime, P0012). Subsequently, equal quantities of protein samples (30 µg) were subjected to SDS-PAGE for separation and then transferred onto PVDF membranes (Millipore, IPVH00010). PVDF were treated with a 5% milk. This was followed by overnight incubation at 4 °C with the antibodies: anti-RUNX2 antibody (Abcam, ab76956, 1:1000), anti-BMP-2 antibody (Abcam, ab14933, 1:1000), anti-PPAR-γ antibody (Abcam, ab178860, dilution 1:1000), anti-C/EBPα antibody (Abcam, ab40761, 1:1000), anti-phospho-p38 MAPK antibody (Abcam, ab4822, 1:1000), anti-HIF-1α antibody (Abcam, ab51608, 1:1000), and anti-GAPDH antibody (Abcam, ab8245, 1:5000) as the internal control. and then were washed with TBST (10 min each) and incubated with HRP- antibodies (Abcam, ab6721, 1:5000) at room temperature for 1 h. After washing three times with TBST, using ECL kit (Beyotime, P0018S) the signals were captured with a gel imaging system.

Quantitative real-time PCR

Total RNA was extracted from BMSC cells by TRIzol reagent and quantified with a NanoDrop 2000 spectrophotometer. qRT-PCR was performed using SYBR

Premix Ex Taq II (Takara, RR820A) on an ABI Prism 7500 Sequence Detection System (Applied Biosystems). Primers for RUNX2, BMP-2, PPAR-γ, C/EBPα, p38 MAPK, HIF-1α, and GAPDH (internal control) were used, with sequences (Table 1).

Statistical analysis

All data are presented as mean ± standard and analyzed using GraphPad Prism 8.3.0 software (GraphPad Software Inc., USA). Unpaired Student's t-tests were used for comparisons between two groups, while one-way analysis of variance (ANOVA) was applied for four groups. $P \leq 0.05$ was deemed significant, * $p < 0.05$, ** $p < 0.01$, *** $p < 0.001$, and **** $p < 0.0001$.

Results

TRFD enhanced the bone microarchitecture in ovariectomized (OVX) mice

We employed microCT to assess femoral trabecular and cortical bone, confirming the effects of TRFD on bone mass. Twelve weeks after ovariectomy, significant improve BMD. All reductions of BMD were significantly reversed following interventions with estradiol (E2) and TRFD (Fig. 2A). The microCT results indicated substantial bone loss in the ovariectomized (OVX) group compared to the sham-operated group, as evidenced by marked decreases in BMD, BV/TV, BS/TV, Tb.Th, Tb.N. Tb.Sp increased significantly ($p < 0.05$). Subsequent administration of TRFD and E2 demonstrated that both treatments reversed bone loss. Compared with OVX group, the OVX+TRFD and E2 groups exhibited significant improvements in bone density, In the treatment of TRFD, the treatment and improvement results of the high-dose TRFD-H group were significantly better than those of the low-dose TRFD-L group, showing a significant dose dependence. BV/TV, BS/TV, Tb.Th, and Tb.N, while Tb.Sp decreased significantly ($p < 0.05$) (Fig. 2B). These findings suggest that ovariectomy reduced bone mass and disrupted bone microarchitecture, whereas treatments with TRFD may mitigate these adverse effects.

TRFD effectively reversed bone histopathological degeneration in ovariectomized (OVX) mice

We conducted an analysis of the metaphyseal of the femur through histomorphology. HE staining demonstrated a complete and intact trabecular structure in the Sham (Fig. 3A). In contrast, OVX exhibited significant trabecular damage, characterized by thinning, fractures, reduced area, and increased trabecular spacing. Following interventions with estradiol E2 and TRFD, these histopathological changes were markedly ameliorated. Specifically, HE is staining showed trabecular structure in the TRFD-treated group was restored, with

Table 1 Primer sequence synthesis

Primer	Primer sequence
RUNX2	CCATCCATCCACTCCACCAC GCCAGAGGCCAGAAGTCAGAG
BMP-2	ACGGAGACACAGCTCACAAG GATCTTCTCCAGGCAGGC
PPAR γ	GGAGCCTAAGTTTGAGTTTGCTGTG TGCAGCAGTTGTCTTGATG
C/EBPα	ATGGCCTGCTGTCGGTG TCACTGCTGGTGATGGTG
p38- AMPK	ACGAAGGAAGAATCCTGTGACAA CAGTCCCTGATTTGGCTTCTGTA
Hif1α	GGACGATGAACATCAAGTCAGCA AGGAATGGGTTTCAAAATCAGCA
GAPDH	AAATGGTGAAGGTGGTGTGAAC CAACAATCTCCACTTTGCCACTG

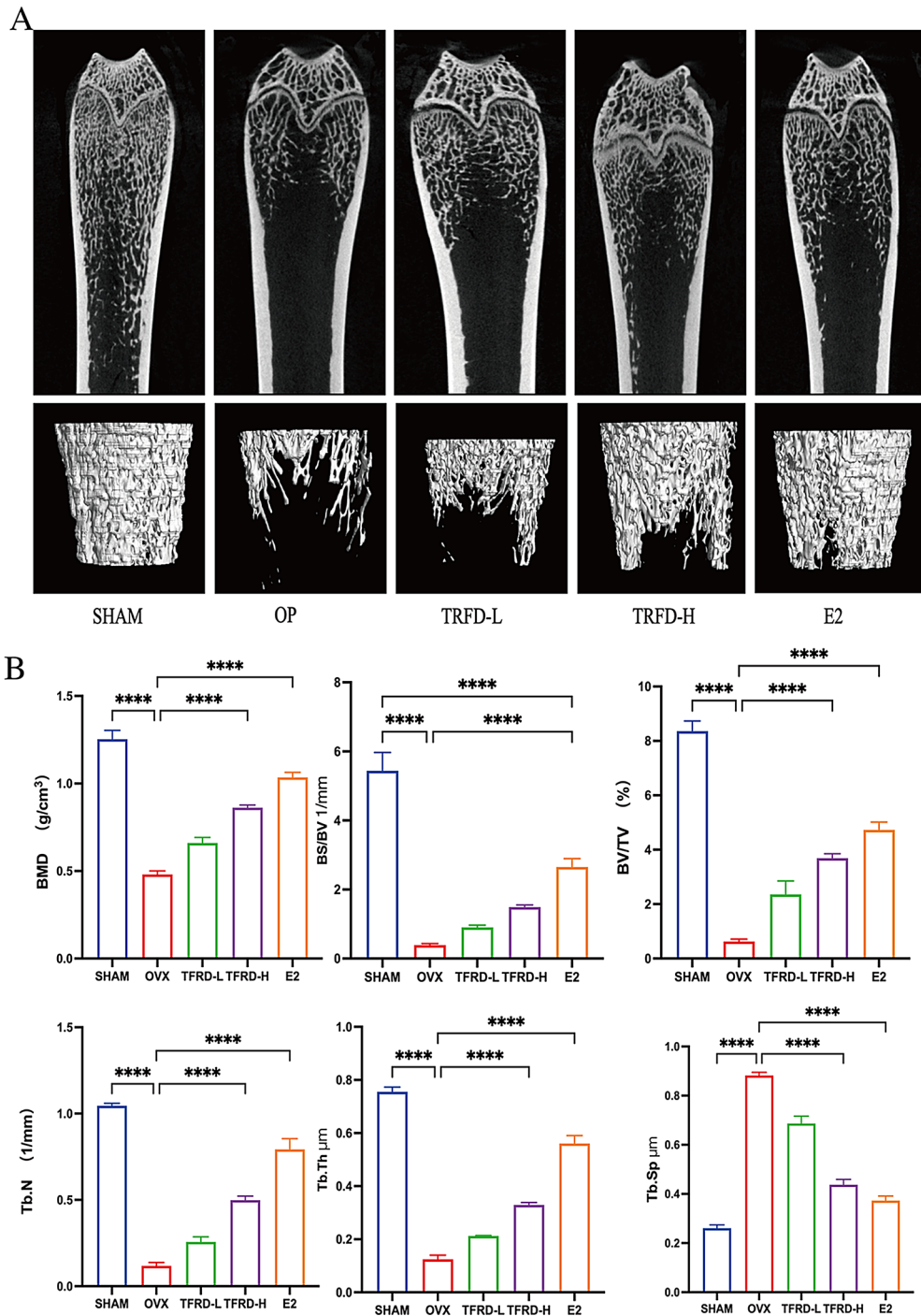


Fig. 2 Micro CT of the femur of mice. **A:** images of micro-CT in each group. **B:**The measured parameters of BMD, BS/TV, BV/TV, Tb.N, Tb.Th, Tb.Sp. mean ± SD, n = 10; *p < 0.05, **p < 0.01, ***p < 0.001, ****p < 0.0001

increased trabecular thickness, reduced trabecular separation, and a more robust and continuous trabecular network compared to the OVX group. TRAP staining demonstrated the osteoclasts in OVX group was significantly higher than SHAM group, indicating an increase in bone resorption (Fig. B). However, the number of osteoclasts was significantly reduced after E2 and TRFD

interventions. In the TRFD-treated group, TRAP staining showed a marked decrease in osteoclast numbers, suggesting reduced bone resorption activity. This reduction in osteoclasts was accompanied by improvements in bone microarchitecture, as evidenced by the restoration of trabecular structure observed in, HE staining. These findings indicate that TRFD effectively reduces

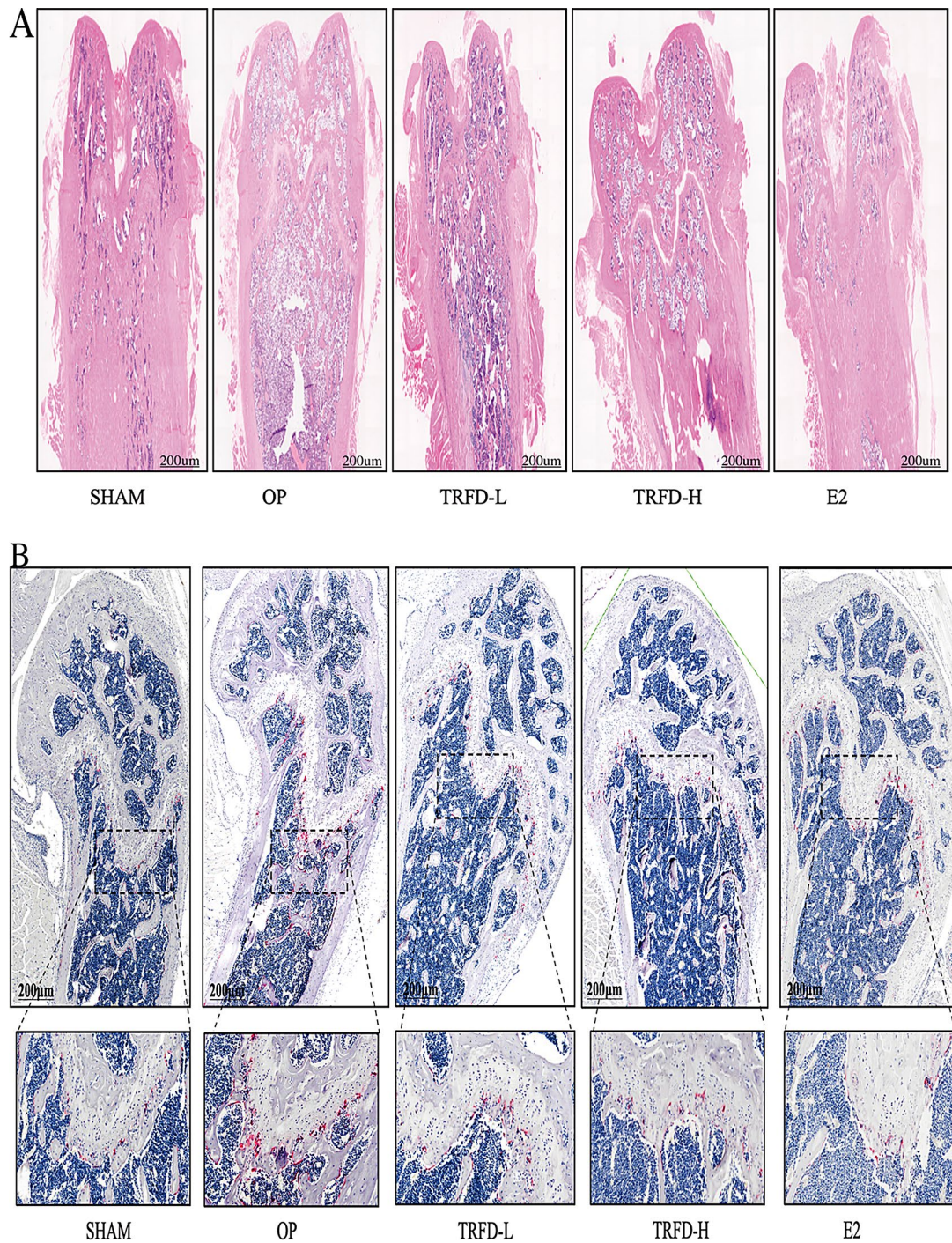


Fig. 3 Histological analysis of the femur was performed for each group. **A:** HE staining, (scale bar 200 μm). **B:** TRAP staining, (active TRAP + osteoclasts stained in red, scale bar 200 μm)

bone resorption and ameliorates bone histopathological changes by inhibiting the activity of osteoclasts. In the treatment of TRFD, the treatment and improvement results of the high-dose TRFD-H group were significantly better than those of the low-dose TRFD-L group, showing a significant dose dependence. The therapeutic efficacy of TRFD in mitigating osteoporosis is likely due

to its ability to modulate osteoclast activity, thereby preserving trabecular structure and bone mass.

TRFD improved the serum markers of bone metabolism and MAPK/HIF-1α in in OVX mice

We employed ELISA kits to detect key markers of osteogenesis activity and measure the content of MAPK and

HIF-1 α . Compared with SHAM group, OVX exhibited severe bone mass loss, significantly decrease in serum RUNX2 and ALP, and low levels of HIF-1 α ,MAPK ($p < 0.05$) (Fig. 4A). Following administration of TRFD and estradiol (E2), both interventions significantly upregulated osteogenesis markers RUNX2 and ALP, increased MAPK content, and elevated HIF-1 α levels ($p < 0.05$) (Fig. 4A). In the treatment of TRFD, the treatment and

improvement results of the high-dose TRFD-H group were significantly better than those of the low-dose TRFD-L group, showing a significant dose dependence. These indicate TRFD effectively improves bone metabolic indices by promoting osteogenesis, enhancing MAPK signaling pathways, and increasing HIF-1 α levels, underscoring its potential as a promising natural treatment for osteoporosis.

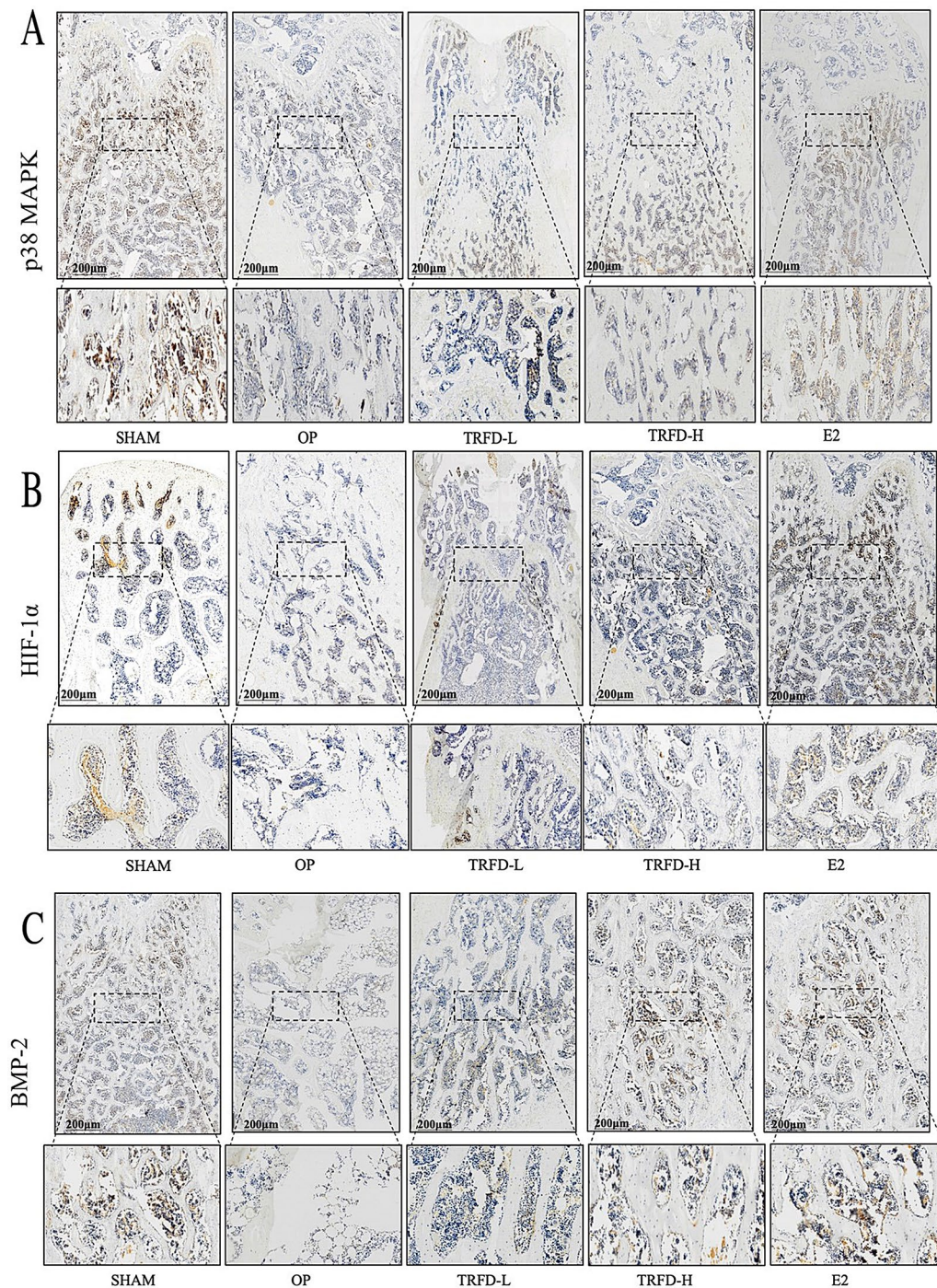


Fig. 4 Immunohistochemistry of femoral tissue of P38-MAPK, HIF-1 α ,BMP-2, (active cell stained brown, scale bar 200 μ m)

TRFD improved expression of osteogenic and adipose with MAPK and HIF-1 α proteins in bone tissue

Immunohistochemistry was used to detect osteogenic proteins and MAPK and HIF-1 α proteins in bone tissue, with positive indicators shown in brown. Compared with SHAM group, OVX group had decreased expression of the osteogenic protein BMP-2, MAPK, and HIF-1 α ($p < 0.05$) (Fig. 4) (Fig. 5B C D), with statistically significant differences ($p < 0.05$) (Fig. 4) (Fig. 5B C D). In the fluorescent staining of bone tissue, positive indicators were stained red. Compared with SHAM group, OVX group exhibited high levels of the adipose marker PPAR- γ . TRFD and E2 were then administered to evaluate their therapeutic effects. Both interventions significantly upregulated the expression of BMP-2, MAPK, and HIF-1 α proteins ($p < 0.05$) (Fig. 4) (Fig. 5B C D). And notably downregulated the content of PPAR- γ ($p < 0.05$) (Fig. 5) (Fig. 6B). Pathological changes after TRFD treatment were notable. TRFD significantly ameliorated bone loss and improved bone microarchitecture in OVX osteoporotic mice. The upregulation of BMP-2 and MAPK indicates enhanced osteogenic differentiation and bone formation, while the increased expression of HIF-1 α suggests improved hypoxic response and cellular adaptation in the bone microenvironment. In the treatment of TRFD, the treatment and improvement results of the high-dose TRFD-H group were significantly better than those of the low-dose TRFD-L group, showing a significant dose dependence ($p < 0.05$) (Fig. 4) (Fig. 5B

C D). Additionally, the elevation of PPAR- γ levels reflects enhanced adipogenic activity ($p < 0.05$) (Fig. 5) (Fig. 6B), which has a destructive effect on maintaining bone marrow homeostasis and overall bone health. In the treatment of TRFD, the treatment and improvement results of the high-dose TRFD-H group were significantly better than those of the low-dose TRFD-L group, showing a significant dose dependence. The results show that E2 and TRFD significantly correcting Bone metabolism indices in OVX osteoporotic mice. TRFD demonstrated a comprehensive therapeutic effect by promoting osteogenesis through the upregulation of BMP-2 and MAPK, enhancing the hypoxic response via reduce the levels of HIF-1 α , and Inhibiting levels of PPAR- γ .

Bioinformatics analysis

Using R software, we performed an intersection analysis of disease target genes and traditional Chinese medicine (TCM) target genes, resulting in a Venn diagram that identified 21 common target genes between TCM and disease (Fig. 7A). Among these, there are 2850 disease target genes and 121 target genes for TRFD. We then applied the DAVID database platform to conduct Gene Ontology (GO) enrichment analysis on the identified potential targets and visualized the results (Fig. 7B, C). The findings indicate that multiple targets are related to pathogenesis of Osteoporosis. The GO enrichment show the core target genes of TRFD primarily involve biological processes related to response to drugs, oxygen levels,

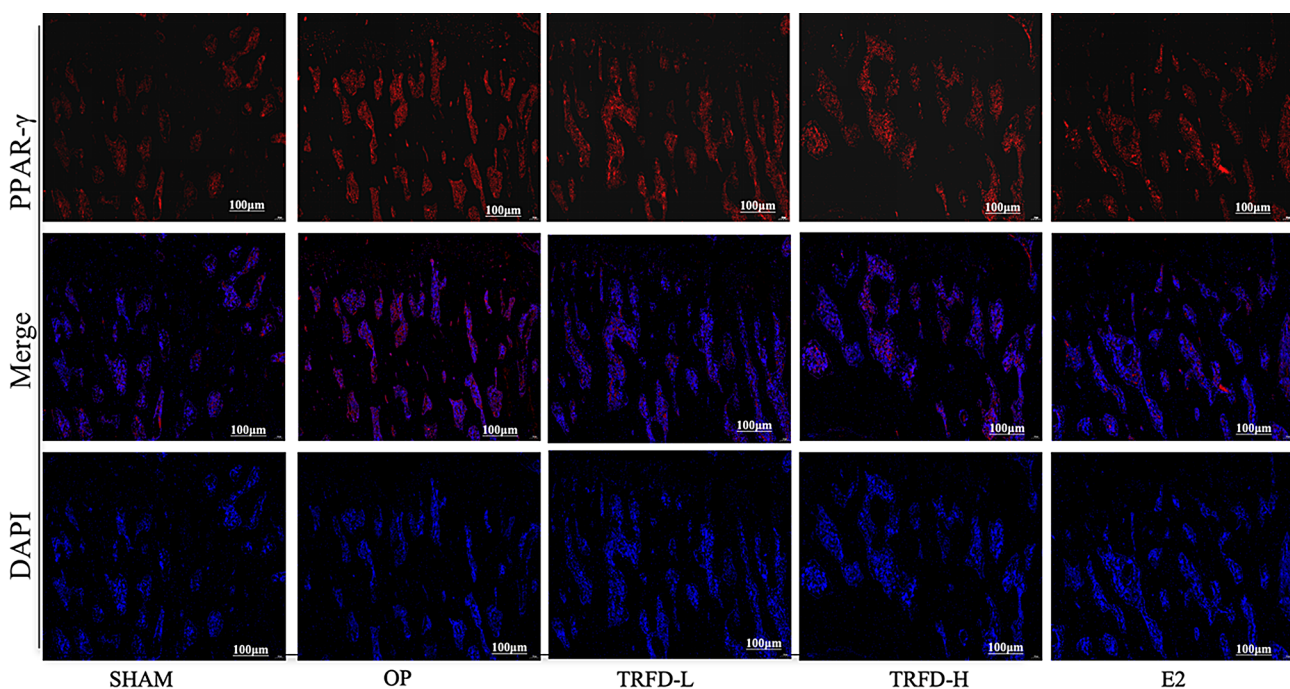


Fig. 5 Immunostaining of femoral from each group, (A) Immunostaining intensity of PPAR γ in femoral tissue, Red signifies cells positive for PPAR γ ; blue DAPI; immunostaining at 40x magnification (scale bar 100 μ m)

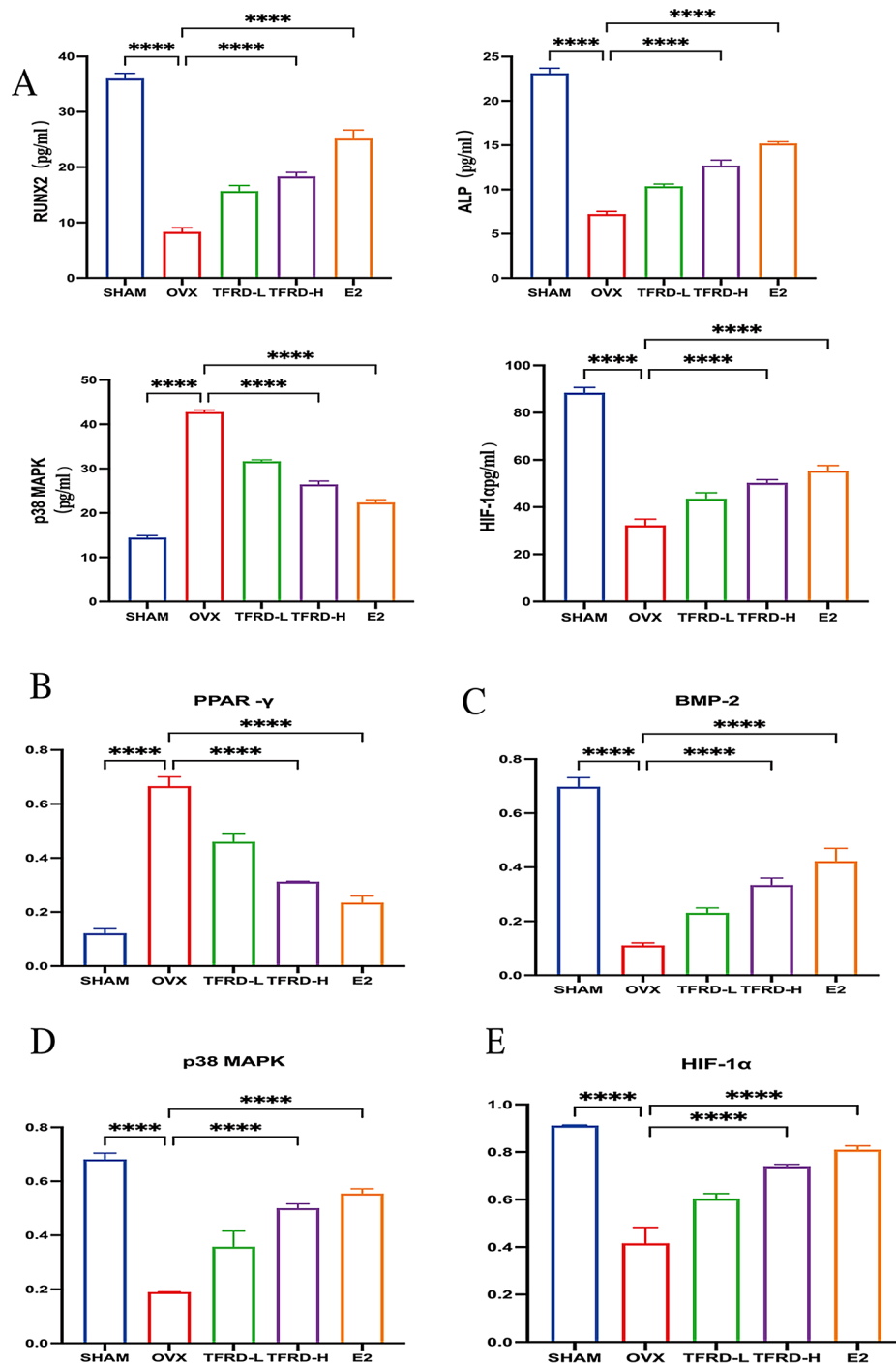


Fig. 6 (A) ELISA for serum RUNX2, ALP, p53MAPK, HIF-1α in each group; (B) Quantitative analysis of Immunostaining staining of PPAR-γ, mean ± SD, n = 10; *p < 0.05, **p < 0.01, ***p < 0.001, ****p < 0.0001; (C), (D), (E) Quantitative analysis of IHC staining of BMP-2, p53MAPK, HIF-1α, mean ± SD, n = 10; *p < 0.05, **p < 0.01, ***p < 0.001, ****p < 0.0001

toxic substances, hypoxia, alkaloids, and decreased oxygen levels, as well as negative regulation of ion transport, negative regulation of calcium ion transport, and aging. In terms of cellular components, these targets mainly act on the nucleus, cytoplasm, and plasma membrane (Fig. 7BC). The molecular functions of the relevant

targets that regulate OP are enriched in protein binding, enzyme binding, and protein homodimerization activity. Important biological processes associated with TRFD include positive regulation of RNA polymerase II promoter transcription, redox processes, negative regulation of apoptosis, and signal transduction. The KEGG

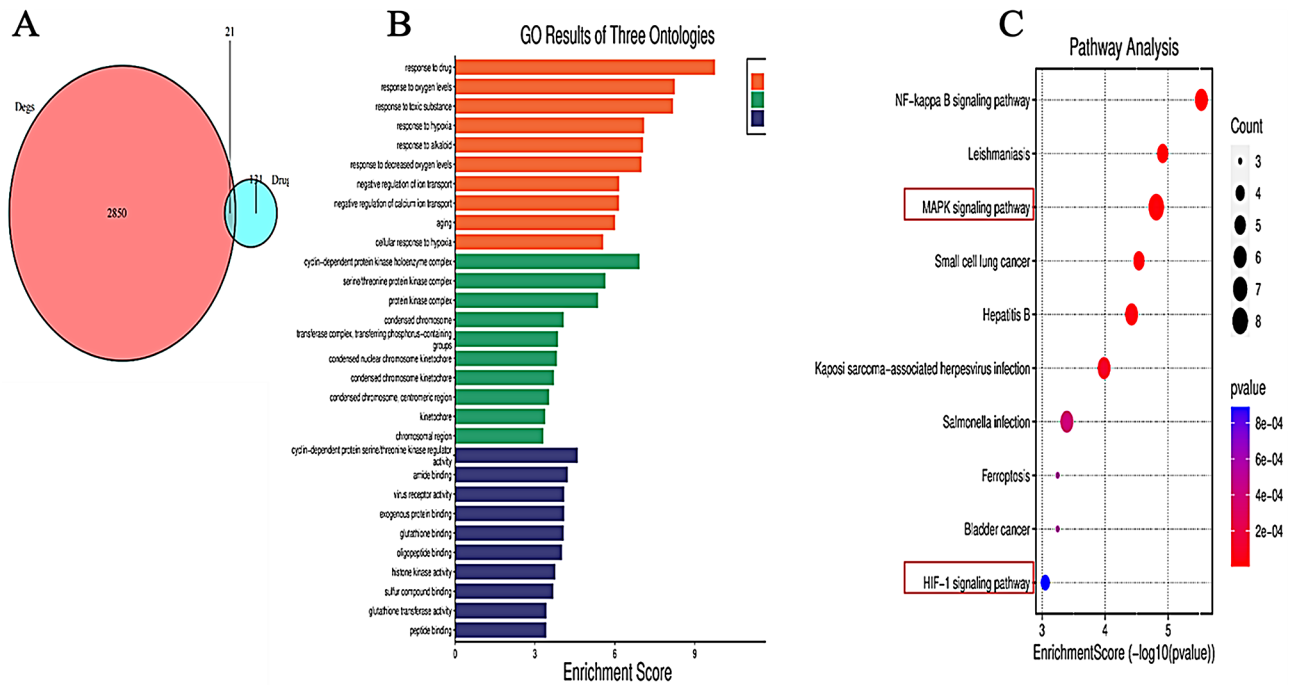


Fig. 7 Bioinformatics analysis diagram (A) Bone fragmentation supplement: drug component-PMOP target, Venn diagram target (B), GO enrichment analysis, bar chart target, (C) KEGG pathway enrichment analysis, bubble map

pathway enrichment analysis results reveal significant involvement of pathways such as, MAPK signaling pathway, small cell lung cancer, Salmonella infection, ferroplois, and HIF-1 signaling pathway. Literature related to osteoporosis signaling pathways indicates that the MAPK signaling pathway, and HIF-1 signaling pathway regulate osteoblasts, osteoclasts, and adipocytes, thereby participating in bone metabolism (Fig. 7B C). The bioinformatics analysis underscores impact of TRFD on gene of expression in primary osteoporosis. The key pathways, particularly the MAPK and HIF-1 signaling pathways, suggests that TRFD may enhance bone microarchitecture by influencing molecular mechanisms associated with bone formation, resorption, and response to stress. These findings show foundation for exploration of TRFD as a therapeutic agent in osteoporosis.

TRFD promotes the BMSC differentiation of osteogenic

ALP activity assay results indicated that the ALP activity in BMSCs cultured with different concentrations of TRFD (1 µg/ml, 10 µg/ml, and 50 µg/ml) was higher than control group ($P < 0.01$), with 50 µg/ml group exhibiting the highest ALP activity ($p < 0.05$) (Fig. 8C). To confirm the effect of TRFD on osteogenic differentiation, 7 days of osteogenic culture, ALP staining of the blank control group showed a light intensity with sparse distribution. In the 1 µg/ml TRFD treatment group, ALP staining was noticeably darker with increased distribution density. The 10 µg/ml TRFD group exhibited even deeper ALP

staining and a larger distribution density, while the 50 µg/ml TRFD group demonstrated the most intense ALP staining and the highest distribution density (Fig. 8B). After 14 days of osteogenic induction, the ARS results were consistent with ALP staining, demonstrating a significant increase in mineralized nodule formation in the TRFD-treated groups (Fig. 8A). The TRFD groups exhibited a significantly greater number of mineralized nodules in BMSC-differentiated osteoblasts compared to the control group. WB highlighted significantly elevated levels of RUNX2 and BMP2 in the TRFD treatment groups ($p < 0.05$) (Fig. 9AB). Furthermore, RT-qPCR results demonstrated a significant increase ($P < 0.05$) in the expression levels of Runx2 and Bmp2 ($p < 0.05$) (Fig. 9C). These suggest TRFD effectively promotes osteogenic differentiation by increased ALP, enhanced mineralization, and elevated expression of key osteogenic markers. The strong correlation between TRFD concentration and the osteogenic response indicates a dose-dependent effect, with higher concentrations yielding greater enhancement of osteogenic differentiation.

TRFD inhibited BMSC differentiation of adipogenesis

On the 14th day after adipogenic induction, Oil Red O staining showed increase the lipid droplets in BMSC-derived adipocytes. Treatment with TRFD of 1, 10, and 50 µg/ml significantly reduced the number of lipid droplets. Compared with adipogenic induction group alone, the areas of ORO-positive regions in the TRFD groups

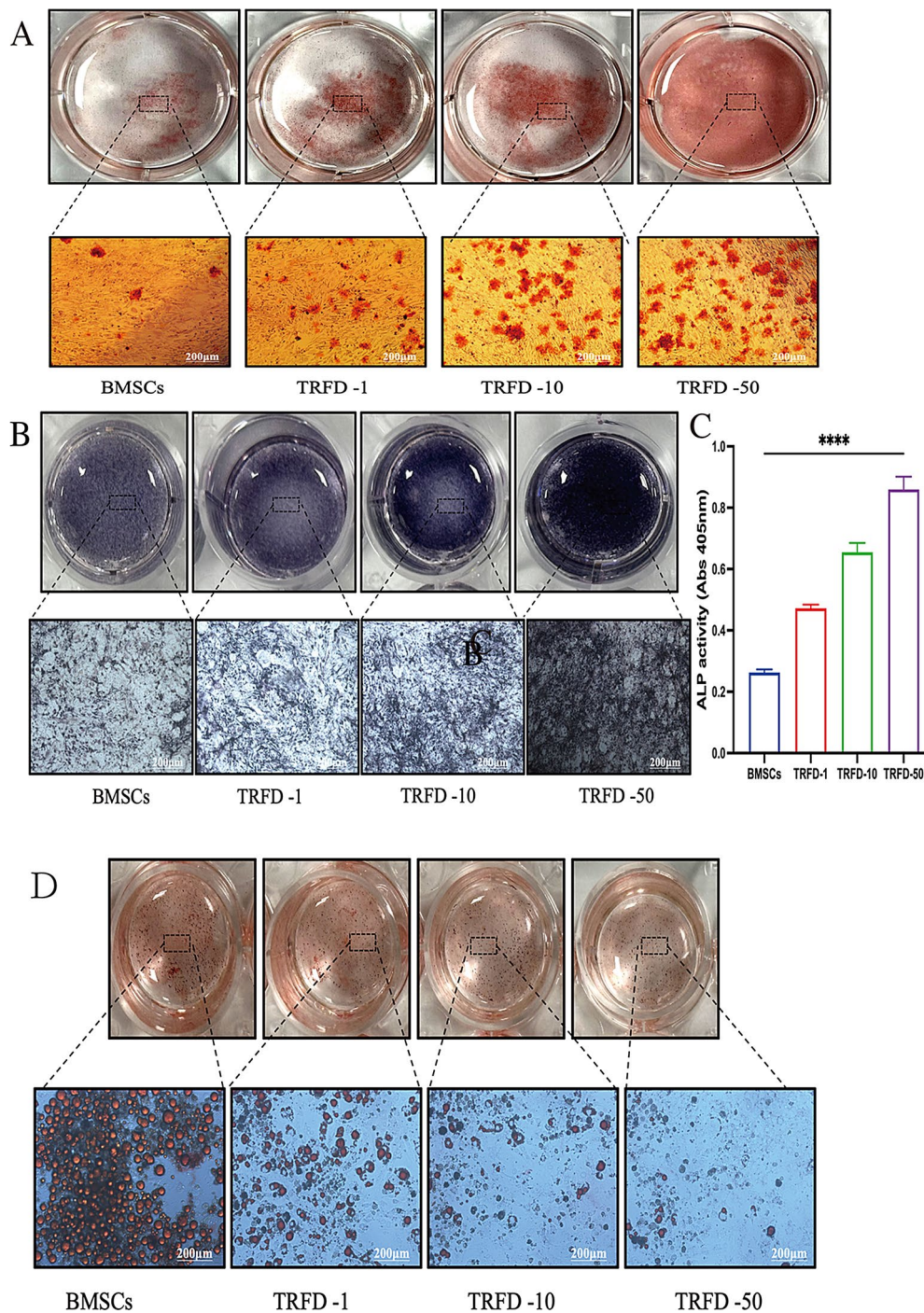


Fig. 8 BMSC osteogenic and adipogenic differentiation. **(A)** Results of alizarin red S staining. **(B)** Results of ALP staining. **(C)** Quantitative results of ALP activity. **(D)** Oil red O staining results, mean ± SD, n = 10; *p < 0.05, **p < 0.01, ***p < 0.001, ****p < 0.0001

were reduced by nearly half, with the 50 µg/ml TRFD treatment showing a significant reduction compared to the BMSCs control group (Fig. 8D). Western blot analysis revealed reduced levels of adipogenesis-related proteins PPAR-γ and C/EBPα. Additionally (p < 0.05) (Fig. 9A B), RT-qPCR results demonstrated a reduction in the expression levels of adipogenesis-related genes PPAR-γ

and C/EBPα, exhibiting a notable dose-dependent effect (p < 0.05) (Fig. 9C). Pathological changes after TRFD treatment were notable. TRFD significantly inhibited adipogenic differentiation of BMSCs, as evidenced by reduced lipid accumulation and decreased expression of key adipogenic markers. The reduction in PPAR-γ and C/EBPα at both protein and gene levels suggests that TRFD

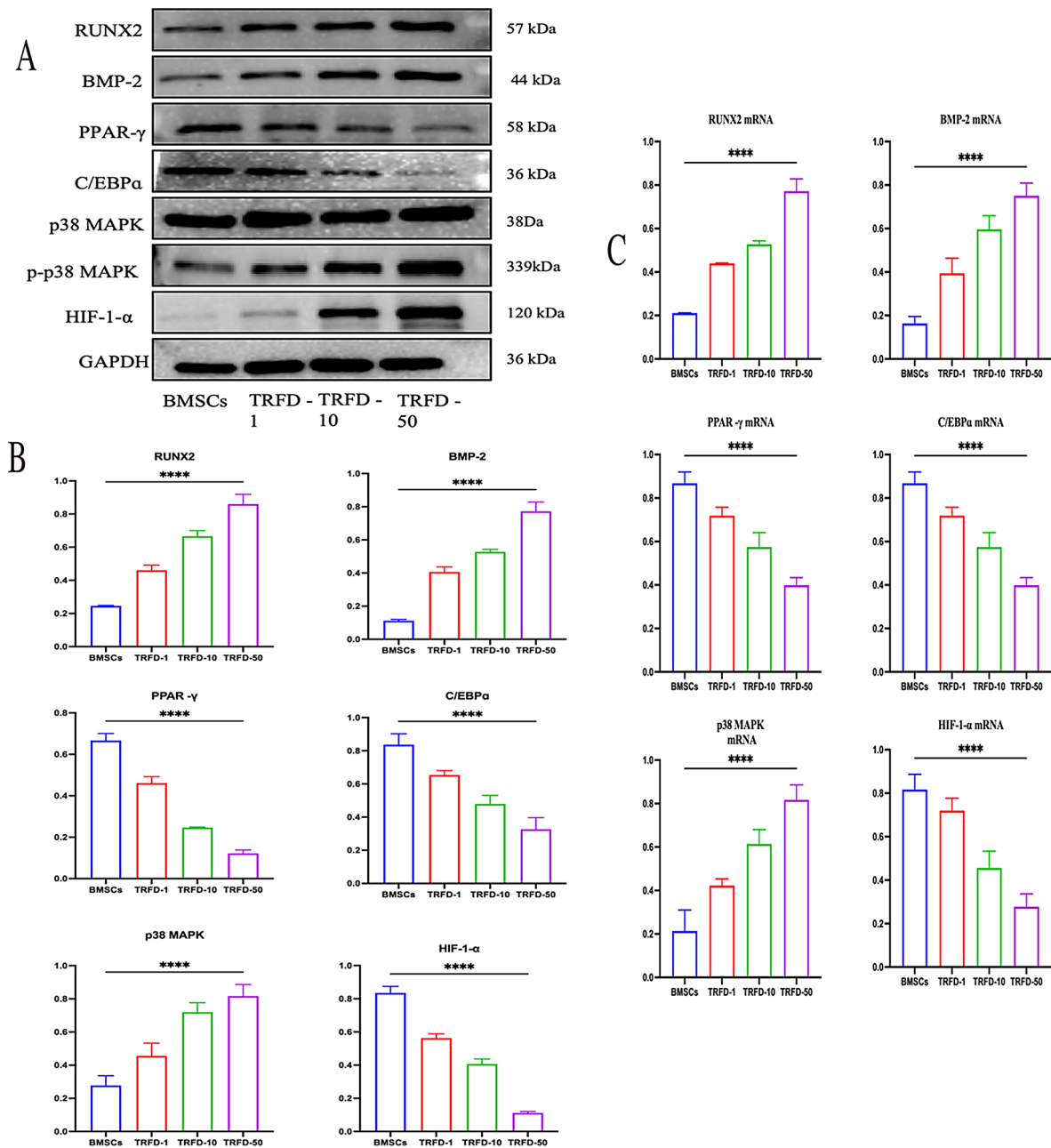


Fig. 9 The expression of key factors MAPK/HIF-1 α , osteogenic markers and adipogenic markers detected using qRT-PCR and Western blot. **(A)** Representative blots showing of Key marker proteins levels. **(B)** Representative graphs showing the relative expression of Key marker proteins. **(C)** Representative graphs of qRT-PCR expression. mean \pm SD, $n = 10$; * $p < 0.05$, ** $p < 0.01$, *** $p < 0.001$, **** $p < 0.0001$

effectively suppresses the adipogenic pathway, thereby potentially reallocating BMSC differentiation towards osteogenesis. This shift in differentiation could be a critical factor in improving bone health and mitigating osteoporotic changes.

TRFD relies on MAPK /HIF-1 α signaling to promoted osteogenesis and inhibited adipogenic expression of BMSC
To gain deeper insights into the MAPK-HIF-1 α pathway in the enhancement of cell differentiation by TRFD,

Under intervention with different concentrations of TRFD (1 μ g/ml, 10 μ g/ml, and 50 μ g/ml), Western blotting analysis and RT-qPCR results indicated that TRFD significantly promoted the phosphorylation of P38-MAPK and markedly increased the expression levels of P38-MAPK compared to the blank control group ($p < 0.05$) (Fig. 9). Concurrently, HIF-1 α protein levels exhibited a notable upregulation. In summary, MAPK-HIF-1 α signaling pathway by TRFD plays a pivotal role in promoting osteogenic differentiation of BMSCs, as

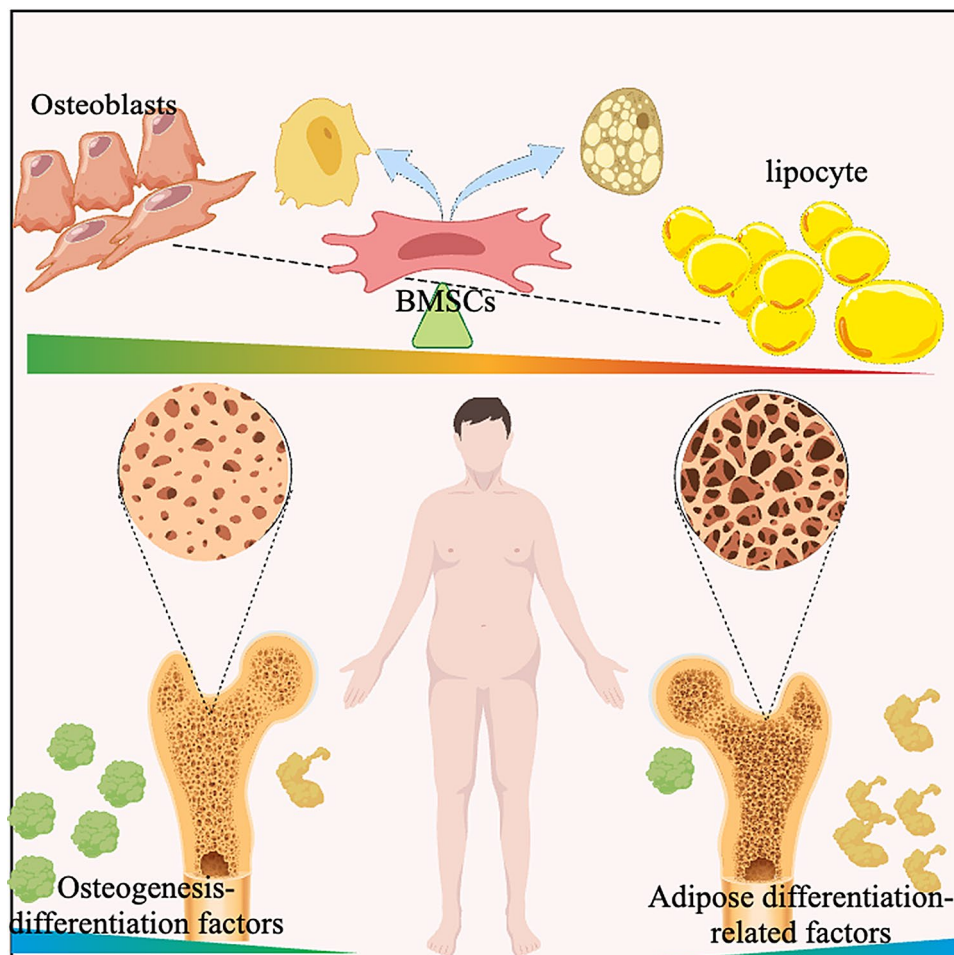


Fig. 10 Summary picture of the research mechanism

evidenced by increased osteogenic marker expression and decreased adipogenic marker levels ($p < 0.05$) (Fig. 9). This dual action of TRFD not only enhances bone formation but also inhibits fat accumulation, as a therapeutic agent for bone metabolic disorders.

Discussion

The pathogenesis of primary osteoporosis [29] is multifactorial, involving a delicate balance between bone resorption and bone formation [7]. Two critical processes, adipogenesis and osteogenesis, play a key role in maintaining balance. osteogenesis involves the transformation of MSCs into osteoblasts, which are the cells that contribute to the formation of bone [30]. The interplay between adipogenesis and osteogenesis is particularly relevant in the context of primary osteoporosis. An increase of osteogenesis within the bone marrow niche is a hallmark of age-related osteoporosis, contributing to reduced bone formation and increased bone fragility (Fig. 10). Understanding the molecular mechanisms that regulate the switch between adipogenic and osteogenic

differentiation is therefore essential for developing targeted therapies for osteoporosis.

Studies have highlighted the importance of MAPK pathway and HIF1- α in regulating both adipogenesis and osteogenesis [31–33]. The MAPK pathway is known to mediate various cellular responses to external stimuli, including stress and growth factors, and has been implicated in the differentiation of MSCs into osteoblasts [34]. On the other hand, HIF1- α , a transcription factor that responds to hypoxic conditions, is crucial in promoting angiogenesis and osteogenesis [35], particularly under low oxygen tension, which is a common feature of the bone marrow microenvironment. BMSCs as a type of stem cell, which exists in bone marrow and cancellous bone. The activated and phosphorylated MAPK signaling pathway regulates BMPs and basic fibroblast growth factor 2, and it is one of the primary pathways involved in osteoblast proliferation and differentiation [36]. The activation of ERK and p38MAPK is directly associated with osteogenesis. Numerous studies have demonstrated that HIF-1 α positively influences BMSCs and significantly promotes their proliferation, migration, and osteogenic

differentiation under conditions of hypoxia. The regulation of HIF-1 α in osteoblasts can be categorized into normoxic and hypoxic conditions. Knockdown of HIF-1 α inhibits osteoblast viability and proliferation under normal oxygen conditions by suppressing the expression of FoxO1 [35]. The decreased level of osteogenic factors, such as Runx2, ALP, also leads to increased levels of ROS and apoptosis. This leads to disordered cortical bone structure and a significant reduction in the bone formation rate and overall bone mass. Marker genes associated with adipogenesis in adipocytes are essential for their function in the formation and function of PPAR γ , C/EBP α , adiponectin, and lipoprotein lipase [37]. PPAR γ as the primary regulatory factors in adipose differentiation, adjusting the formation of adipocytes, lipid storage, and insulin sensitivity [38]. This process is activated by multiple genes related to lipid metabolism, promoting the differentiation of precursor cells into mature adipocytes. C/EBP α is another crucial transcription factor that, in conjunction with PPAR γ , cooperates to regulate the differentiation process of adipocytes. C/EBP α plays a significant role in the early stages of adipogenic differentiation, assisting in the maintenance of the terminally differentiated state of adipocytes [39, 40].

Research has indicated that TRFD can influence the activity, and differentiation of bone cells via various mechanisms. These effects contribute to enhanced bone formation, reduced bone resorption, and offer potential benefits. Studies have indicated that *Drynaria* total flavonoids possess estrogen-like effects and can treat osteoporosis by reducing the expression of osteoclasts in bone tissue and increasing the mineral content of femoral bone in ovariectomized female rats. Li Yan et al. found that *Dryfill* inhibited the mRNA expression of PPAR γ and LPL, subsequently inhibiting the adipogenic differentiation of rat BMSCs, increasing bone mineral density in rats, and contributing to its anti-osteoporosis effects. In this study, we utilized an ovariectomized mouse model to evaluate the therapeutic potential of TRFD in modulating bone microarchitecture, bone metabolism markers, and the differentiation of BMSCs into osteogenic and adipogenic lineages. Our comprehensive experimental analysis confirmed the efficacy of TRFD in ameliorating postmenopausal osteoporosis. Micro-CT showed significant trabecular bone loss and deterioration in the OVX group, characterized by reductions in BV/TV, BS/TV, Tb.Th, and Tb.N, accompanied by increased Tb.Sp. However, the administration of TRFD significantly reversed these detrimental changes, demonstrating its protective effect on bone microarchitecture by mitigating bone loss. Histomorphometric analysis and TRAP staining further corroborated the protective effects of TRFD. OVX mice exhibited marked histopathological deterioration, including trabecular thinning, fractures, and an increase

in osteoclast numbers. TRFD treatment significantly reduced osteoclast activity and improved trabecular integrity, suggesting that TRFD exerts its anti-osteoporotic effects by inhibiting excessive osteoclast. ELISA and immunohistochemistry demonstrated that TRFD significantly upregulated osteogenesis-related markers, such as RUNX2 and BMP-2. Concurrently, TRFD promoted the activation of the MAPK and HIF-1 α . These results indicate that TRFD facilitates osteogenic differentiation by modulating the MAPK/HIF-1 α signaling axis, which plays a pivotal role in the regulation of bone metabolism.

It is noteworthy that most current studies focus on the imbalance between osteogenesis and osteoclastogenesis, whereas our study specifically investigates the correlation between osteogenic and adipogenic differentiation of BMSCs. In our study, the effect of TRFD on BMSC differentiation was treated through Oil Red staining, ALP activity assays, staining and PCR and Western blot analysis. TRFD significantly inhibited adipogenic differentiation, as evidenced by decreased lipid droplet formation and reduced expression of adipogenesis-associated proteins, including PPAR- γ and C/EBP α . Conversely, TRFD enhanced osteogenic differentiation, as indicated by increased ALP activity, mineralized nodule formation, and upregulation of osteogenic proteins such as RUNX2 and BMP-2. These findings underscore the role of TRFD in directing BMSC differentiation toward the osteogenic lineage while concurrently inhibiting adipogenesis. In addition, we have also demonstrated the mechanism and regulatory role of MAPK/HIF-1 α pathway in the process of osteogenic adipogenic differentiation through in vitro cell experiments, and bioinformatics analysis has also obtained relevant pathway. The analysis revealed that TRFD targets critical signaling pathways implicated in the pathogenesis of PMOP, including NF- κ B, MAPK, and HIF-1 pathways, which are integral to the regulation of osteoblast, osteoclast, and adipocyte activity in bone metabolism.

In summary, our study provides compelling evidence that TRFD exerts a multifaceted protective effect against bone loss in OVX-induced osteoporotic mice. TRFD not only restores bone microarchitecture and modulates key bone metabolism markers but also promotes osteogenesis while inhibiting adipogenesis through the regulation of the MAPK/HIF-1 α pathway. These results indicate TRFD can be a promising therapeutic option for managing postmenopausal osteoporosis. Further studies are needed to assess the clinical safety and effectiveness of TRFD to determine its applicability in human treatments.

Conclusion

In all, this study highlights the significant therapeutic potential of TRFD in the management of osteoporosis. TRFD effectively promotes osteogenesis and inhibits

adipogenesis in mesenchymal stem cells, evidenced by improved bone microarchitecture and enhanced serum osteogenic markers in ovariectomized mice. As shown in this study, MAPK and HIF-1 α signaling pathways are crucial in mediating these effects. These results indicate that TRFD can be a valuable natural treatment for osteoporosis, warranting further exploration into its mechanisms and clinical applications.

Abbreviations

TRFD	Total flavonoids of <i>Rhizoma Drynariae</i> (<i>Drynaria fortunei</i> J. Smith)
OP	Osteoporosis
BMSCs	Bone marrow mesenchymal stem cells
Runx2	Runt-related transcription factor 2
BMP-2	Bone Morphogenetic Protein-2
TGF- β	Transforming growth factor β
PPAR γ	Peroxisome proliferator-activated receptor γ
C/EBP α	CCAAT/enhancer-binding protein α
TFDR	Total flavonoids of <i>rhizoma drynariae</i>
ALP	Alkaline phosphatase
MAPK	Mitogen-activated protein kinase
HIF1- α	Hypoxia-Inducible Factor 1- α
TRAP	Tartrate-resistant acid phosphatase
HE	Hematoxylin and eosin
SHAM	Sham-operated group
OVX	The ovariectomized group
GO	Gene Ontology
ROS	Reactive oxygen species
BMD	Bone mineral density
BS	Bone Surface
BV	Bone Volume
TV	Tissue Volume
Tb.sp	Trabecular Separation/Spacing
qRT-PCR	Quantitative Real-time PCR

Author contributions

Hui su, Luyao Liu: Complete the manuscript writing. Rujie Zhuang: Complete the manuscript revised. All the authors have read and approved the final manuscript. Luyao Liu, Zechen Yan: contributed significantly to the experiments, and analysis. Yu Pan: conceived and designed the experiments.

Funding

This project was sponsored by the Zhejiang Chinese Medical University Scientific Research Fund Project (Project Number: No. 2023FSYYZQ03); Zhejiang Province Traditional Chinese Medicine Science and Technology Project (Project Number: No. 2023ZL038, NO. 2025ZR122); Quzhou Science and Technology Plan Project 2023K155; National Natural Science Foundation of China (82174410); The funders had no role in study design, data collection and analysis, decision to publish, or preparation of the manuscript.

Data availability

No datasets were generated or analysed during the current study.

Declarations

Ethics, consent to participate, and consent to publish

Not applicable.

Competing interests

The authors declare no competing interests.

Author details

¹The First School of Clinical Medicine, Zhejiang Chinese Medical University, Hangzhou, Zhejiang Province 310053, China

²Orthopedic Department, The First Affiliated Hospital of Zhejiang Chinese Medical University (Zhejiang Provincial Hospital of Traditional Chinese Medicine), Hangzhou 310053, China

³Department of Pharmacy, Tianjin First Central Hospital, Tianjin 300000, China

⁴Quzhou TCM Hospital at the Junction of Four Provinces Affiliated to Zhejiang Chinese Medical University, Quzhou 324000, China

Received: 11 February 2025 / Accepted: 27 February 2025

Published online: 11 March 2025

References

1. Fuggle NR, Beaudart C, Bruyère O, Abrahamsen B, Al-Daghri N, Burlot N, et al. Evidence-Based guideline for the management of osteoporosis in men. *Nat Rev Rheumatol*. 2024;20(4):241–51.
2. Andersen MØ, Andresen AK, Hartvigsen J, Hermann AP, Sørensen J, Carreon LY. Vertebroplasty for painful osteoporotic vertebral compression fractures: a protocol for a single-center double-blind randomized sham-controlled clinical trial. *VOPE2*. *J Orthop Surg Res*. 2024;19(1):813.
3. Foessel I, Dimai HP, Obermayer-Pietsch B. Long-term and sequential treatment for osteoporosis. *Nat Rev Endocrinol*. 2023;19(9):520–33.
4. Bao X, Liu C, Liu H, Wang Y, Xue P, Li Y. Association between polymorphisms of glucagon-like peptide-1 receptor gene and susceptibility to osteoporosis in Chinese postmenopausal women. *J Orthop Surg Res*. 2024;19(1):869.
5. Leeyaphan J, Rojjananukulpong K, Intarasompan P, Peerakul Y. Simple clinical predictors for making directive decisions in osteoporosis screening for women: a cross-sectional study. *J Orthop Surg Res*. 2024;19(1):789.
6. Huang F, Wang Y, Liu J, Cheng Y, Zhang X, Jiang H. Asperuloside alleviates osteoporosis by promoting autophagy and regulating Nrf2 activation. *J Orthop Surg Res*. 2024;19(1):855.
7. Lewiecki EM, Czerwinski E, Recknor C, Strzelecka A, Valenzuela G, Lawrence M, et al. Efficacy and safety of transdermal abaloparatide in postmenopausal women with osteoporosis: A randomized study. *J Bone Min Res*. 2023;38(10):1404–14.
8. Qaseem A, Mount CA, Campos K, McLean RM, Tierney S, Cross JT Jr, et al. Quality indicators for osteoporosis in adults: A review of performance measures by the American college of physicians. *Ann Intern Med*. 2023;176(10):1386–91.
9. Morin SN, Feldman S, Funnell L, Giangregorio L, Kim S, McDonald-Blumer H, et al. Clinical practice guideline for management of osteoporosis and fracture prevention in Canada: 2023 update. *CMAJ*. 2023;195(39):E1333–48.
10. Eisenstein A, Chitalia SV, Ravid K. Bone marrow and adipose tissue adenosine receptors effect on osteogenesis and adipogenesis. *Int J Mol Sci*. 2020;21(20).
11. Yoshida M, Nakashima A, Ishiuchi N, Miyasako K, Morimoto K, Tanaka Y et al. Comparison of the therapeutic effects of Adipose- and bone Marrow-Derived mesenchymal stem cells on renal fibrosis. *Int J Mol Sci*. 2023;24(23).
12. Naji A, Eitoku M, Favier B, Deschaseaux F, Rouas-Freiss N, Suganuma N. Biological functions of mesenchymal stem cells and clinical implications. *Cell Mol Life Sci*. 2019;76(17):3323–48.
13. Brown C, McKee C, Bakshi S, Walker K, Hakman E, Halassy S, et al. Mesenchymal stem cells: cell therapy and regeneration potential. *J Tissue Eng Regen Med*. 2019;13(9):1738–55.
14. Futrega K, Mosaad E, Chambers K, Lott WB, Clements J, Doran MR. Bone marrow-derived stem/stromal cells (BMSC) 3D microtissues cultured in BMP-2 supplemented osteogenic induction medium are prone to adipogenesis. *Cell Tissue Res*. 2018;374(3):541–53.
15. Dang J, Yang J, Yu Z, Chen L, Zhang Z, Wang K, et al. Bone marrow mesenchymal stem cells enhance angiogenesis and promote fat retention in fat grafting via polarized macrophages. *Stem Cell Res Ther*. 2022;13(1):52.
16. Aaron N, Kraakman MJ, Zhou Q, Liu Q, Costa S, Yang J et al. Adipsin promotes bone marrow adiposity by priming mesenchymal stem cells. *Elife*. 2021;10.
17. Zhou X, Cao H, Guo J, Yuan Y, Ni G. Effects of BMSC-Derived EVs on bone metabolism. *Pharmaceutics*. 2022;14(5).
18. Chen GY, Liu XY, Yan XE, Yu X, Liu Y, Luo J, et al. Total flavonoids of *rhizoma drynariae* treat osteoarthritis by inhibiting arachidonic acid metabolites through AMPK/NF κ B pathway. *J Inflamm Res*. 2023;16:4123–40.
19. Gil TY, Park J, Park YJ, Kim HJ, Cominguez DC, An HJ. *Drynaria rhizome* water extract alleviates high-fat diet-induced obesity in mice. *Mol Med Rep*. 2024;29(2).
20. Xiaolong M, Tao Z, Na L. Research progress on the mechanism of osteoclastic repair in the treatment of traumatic fractures. *Mod Med Clin Pract*. 2022;37(10):2386–9.

21. Chengzhi S. Experimental research progress on the mechanism of *Drynaria* total flavonoids in the treatment of osteoporosis. *Chin J Traditional Chin Med*. 2010;28(06):1272–4.
22. Guoqing D, Fuwei P, Yupeng W, jade, Sg, Zhengyan L, honest Tb et al. Meta-analysis of the efficacy and safety of Qianggu capsule in the treatment of primary osteoporosis. *Traditional Chinese medicine bone setting*. 2023;35(08):31–6.
23. Jin X. To observe the effect of Qianggu capsule combined with alendronate sodium in the treatment of senile osteoporosis and its influence on bone metabolism indexes. *Famous Doctors*. 2022(09):159–61.
24. Lin H, Wang X, Li Z, Huang M, Feng J, Chen H, et al. Total flavonoids of rhizoma *drynariae* promote angiogenesis and osteogenesis in bone defects. *Phytother Res*. 2022;36(9):3584–600.
25. Shen Z, Chen Z, Li Z, Zhang Y, Jiang T, Lin H, et al. Total flavonoids of rhizoma *drynariae* enhances Angiogenic-Osteogenic coupling during distraction osteogenesis by promoting type H vessel formation through PDGF-BB/PDGFR- β instead of HIF-1 α /VEGF Axis. *Front Pharmacol*. 2020;11:503524.
26. Chen D, Chu F, Zhang G, Wang Q, Li Y, Zhang M et al. 12-Deoxyphorbol 13-acetate inhibits RANKL-induced osteoclastogenesis via the Attenuation of MAPK signaling and NFATc1 activation. *Int Immunopharmacol*. 2021;101(Pt A):108177.
27. Lin X, Wang Y, Guo X, Li C, Wu K, Wang S, et al. Shikonin promotes rat periodontal bone defect repair and osteogenic differentiation of BMSCs by p38 MAPK pathway. *Odontology*. 2023;111(3):649–57.
28. Han BK, Yoon H, Kim KH, Shin EC, Ko KS, Lee HS, et al. Inhibitory effects of wheat sprouts extract on RANKL-Induced osteoclast differentiation via suppressing MAPK and NFATc1 signaling pathways. *J Med Food*. 2023;26(7):480–8.
29. Zhang J, Hu W, Zou Z, Li Y, Kang F, Li J, et al. The role of lipid metabolism in osteoporosis: clinical implication and cellular mechanism. *Genes Dis*. 2024;11(4):101122.
30. Gorga A, Rindone GM, Dasso ME, Centola CL, Pellizzari EH, Camberos MC, et al. Simultaneous regulation of lactate production and fatty acid metabolism by Resveratrol in rat Sertoli cells. *Biochimie*. 2023;208:75–85.
31. Xiao J, Han Q, Yu Z, Liu M, Sun J, Wu M et al. Morroniside inhibits inflammatory bone loss through the TRAF6-Mediated NF- κ B/MAPK signalling pathway. *Pharmaceuticals (Basel)*. 2023;16(10).
32. Bie M, Tang Y, Xia Y, Zhang Q, Tian Y, Cheng C, et al. HIF-1 α mediates osteoclast-induced disuse osteoporosis via cytoophidia in the femur of mice. *Bone*. 2023;168:116648.
33. Wang H, Kaplan FS, Pignolo RJ. The HIF-1 α and mTOR pathways amplify heterotopic ossification. *Biomolecules*. 2024;14(2).
34. Wang D, Liu L, Qu Z, Zhang B, Gao X, Huang W, et al. Hypoxia-inducible factor 1 α enhances RANKL-induced osteoclast differentiation by upregulating the MAPK pathway. *Ann Transl Med*. 2022;10(22):1227.
35. Lee SY, Kim SJ, Park KH, Lee G, Oh Y, Ryu JH, et al. Differential but complementary roles of HIF-1 α and HIF-2 α in the regulation of bone homeostasis. *Commun Biol*. 2024;7(1):892.
36. Sun K, Zhu J, Deng Y, Xu X, Kong F, Sun X, et al. Gamabufotalin inhibits osteoclastogenesis and counteracts Estrogen-Deficient bone loss in mice by suppressing RANKL-Induced NF- κ B and ERK/MAPK pathways. *Front Pharmacol*. 2021;12:629968.
37. Liu C, Xiong Q, Li Q, Lin W, Jiang S, Zhang D, et al. CHD7 regulates bone-fat balance by suppressing PPAR- γ signaling. *Nat Commun*. 2022;13(1):1989.
38. Fan J, Zhang D, Jiang Y, Yu L, Han B, Qian Z. The effects of PPAR γ inhibitor on bones and bone marrow fat in aged glucocorticoid-treated female rats. *Exp Gerontol*. 2023;181:112281.
39. Kim Y, Ji H, Ryu D, Cho E, Park D, Jung E. *Albizia julibrissin* exerts Anti-Obesity effects by inducing the Browning of 3T3L1 white adipocytes. *Int J Mol Sci*. 2023;24(14).
40. Li XF, Yin SQ, Li H, Yang YL, Chen X, Song B, et al. PPAR- γ alleviates the inflammatory response in TNF- α -induced fibroblast-like synoviocytes by binding to p53 in rheumatoid arthritis. *Acta Pharmacol Sin*. 2023;44(2):454–64.

Publisher's note

Springer Nature remains neutral with regard to jurisdictional claims in published maps and institutional affiliations.